*J. Phys. Chem. A* **1998,** *102,* 7549−7557

# Excitation Effects on the Quantum Dynamics of Two-Dimensional Photoinduced Nonadiabatic Processes

**John M. Jean**[†]

*Department of Chemistry, Washington University, St. Louis, Missouri 63130*

*Received: March 18, 1998; In Final Form: June 24, 1998*

Results are presented from quantum dynamical simulations of vibrationally coherent condensed phase electronic surface crossing processes that take into account the relative positions of the ground, reactant, and product excited states. We find that the degree of Franck−Condon activity in the various vibrational modes can have a significant effect on the surface crossing probability, the nature and magnititude of coherent surface recrossings, and the nature of vibrational motion in the product state when motion in the reactant well is underdamped. The results are discussed in the context of recent femtosecond studies of the photodissociation of the myoglobin−nitric oxide complex and the photoisomerization of the retinal prosthetic group in the rhodopsin system.

## Introduction

The use of femtosecond pump−probe techniques to prepare and detect coherent vibrational wave packets on excited-state surfaces has provided new insight into the role of coherent vibrational dynamics in ultrafast electronically nonadiabatic processes.[1−23] For a dipole-allowed transition, impulsive excitation results in a wave packet localized in the Franck−Condon region of the upper surface, which subsequently moves out along the Franck−Condon directions. In condensed phases, dissipative interactions with other intramolecular and/or solvent motions lead to a rapid loss of phase coherence among the nuclear eigenstates that make up the wave packet. If the dephasing process is complete before the wave packet can travel from the Franck−Condon region of the upper surface to the surface crossing region, then the decay of population in the initially excited state is monotonic and observation of the electronic state population dynamics provides little direct information on the nature of the reactive nuclear motion. If complete thermalization with the environment occurs on a time scale that is short compared to the reaction, then classical and semiclassical methods can be used to compute the equilibrium rate of barrier crossing.[24−26] In this case, the decay of electronic population in the intially excited state is independent of the nature of the excitation process.

If the dissipative interactions are sufficiently weak that the nuclear motion in the reactant well is underdamped, the wave packet may repetitively sample the region where the reactant and product diabatic surfaces cross. Each visit of the reactant-state wave packet to the crossing region results in a fraction of the wave packet being launched on the product surface, giving rise to the possibility of stepwise decay of the reactant population. If the nuclear motion in the product well is underdamped, the wave packet can revisit the surface crossing region, resulting in electronic recurrences (coherent barrier recrossings). These processes are illustrated schematically in Figure 1.

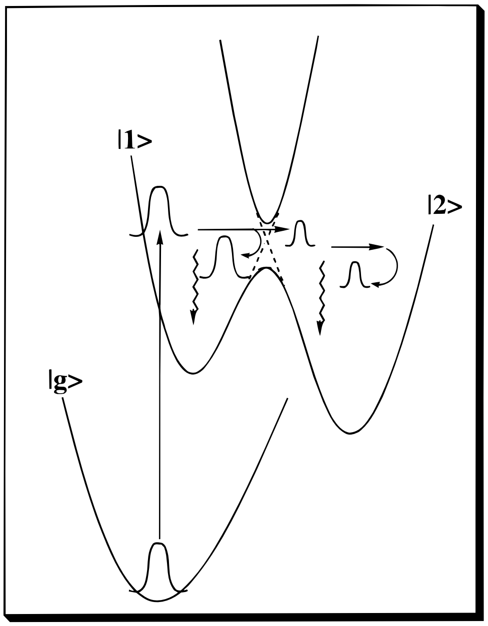

**Figure 1.** One-dimensional electronically nonadiabatic process illustrating the competition between coherent electronic curve crossings, recrossings, and dissipative dynamics. Labels refer to the diabatic surfaces.

To the extent that the reactant and product states are spectrally distinct, information on electronic population dynamics can be obtained by integrating the probe signal over wavelength. Displacement of the final surface in the probe process along one or more of the modes that couple to the curve crossing process leads to a mapping of the time-evolving spatial probability onto the spectral dynamics. When this is the case, information on reactant and/or product wave packet motion can be obtained by frequency resolving the probe signal.

Recent time-resolved experiments have detected vibrationally coherent products following ultrafast nonadiabatic processes in a variety of systems. For example, Apkarian and co-workers,[6,7] in their studies of $I_2$ photodissociation in solid rare gas matrices, observed coherent oscillations in the ground state of $I_2$ resulting from geminate recombination. Wynne et al.[13,14] have shown that coherent vibrational dynamics strongly influence the excited-state charge-transfer process in the TCNE−pyrene

---

[†] Present address: Department of Biochemistry and Molecular Biophysics, Washington University School of Medicine, St. Louis, Missouri 63110.

S1089-5639(98)01553-9 CCC: $15.00

complex. Coherent nuclear dynamics accompanying excited-state processes have also been observed in several chromophore–protein complexes. Zhu et al.[11] observed coherent iron–histidine stretching and heme-doming dynamics in the ground state of myoglobin following photodissociation of the myoglobin–NO complex. Mathies, Shank, and co-workers[15–18] have shown that the isomerization of 11-*cis*-retinal in the visual pigment rhodopsin occurs irreversibly in less than 200 fs, leading to a trans photoproduct that is formed vibrationally coherent in a 60-cm$^{-1}$ skeletal torsion motion. A recent multimode wave packet analysis of this process by Wexler and Mathies based on resonance Raman intensities suggests that the wave packet actually reaches the crossing region in $<$50 fs.[27] These studies are significant in that they provide clear evidence in each case of the nature of the nuclear motions that couple to the electronic process and demonstrate that models based on diffusive nuclear motion do not adequately describe these nonadiabatic processes.

A proper theoretical description of ultrafast electronically nonadiabatic processes requires explicitly treating both the optical preparation step and the ensuing nonstationary vibrational dynamics. In a series of recent papers, we[28–31] and others[32–36] have developed multilevel Redfield theory into a powerful tool for investigating the interplay of electronic and vibrational coherences and dissipative dynamics in ultrafast electronic processes. Our simulations of nonadiabatic dynamics in one-dimensional, three-state model systems have shown that wave packets launched on the reactant surface can survive nonadiabatic curve crossing processes, giving rise to vibrationally coherent products and the possibility of coherent surface recrossings. Results from these studies have also demonstrated the importance of non-Bloch (e.g., bath-induced coherence transfer) processes in electronically nonadiabatic reactions. In addition, we have used this approach to show how one can use time- and frequency-resolved fluorescence to disentangle electronic and nonstationary vibrational dynamics in systems undergoing ultrafast charge-transfer reactions. Similar studies have been carried out recently by Bixon and Jortner using a somewhat different theoretical approach.[37]

In one-dimensional models, the initial force acting on the wave packet is necessarily directed along the reactive motion. In many systems of chemical interest, however, several vibrations strongly couple to both the optical excitation and nonadiabatic transitions. In such cases, impulsive excitation of two or more of these modes leads to an evolving multidimensional wave packet. The initial location of the wave packet on the upper surface will depend on both the nuclear coordinate displacements between ground and reactant excited state and on the spectral and temporal properties of the excitation pulse. The short-time nuclear dynamics accompanying the electronic surface crossing process will be governed in large part by the extent to which the Franck–Condon active modes project onto the motions that couple to the nonadiabatic process (i.e., reactive modes). For example, in the rhodopsin system, the reactive skeletal torsion motion is strongly Franck–Condon active in the $S_1 \leftarrow S_0$ transition of the 11-*cis*-retinal prosthetic group due to the steric repulsion between the 13-methyl group and the 10-hydrogen. Impulsive excitation of this mode thus produces a vibrational wave packet that experiences a significant force in the direction of the cis–trans surface crossing region, which accounts for the ultrafast nature of the isomerization process and the formation of a vibrationally coherent trans photoproduct. Multidimensional coherence effects may also play a critical role in determining the rapid and irreversible nature of the isomerization process in the rhodopsin system by effectively directing the nascent product wave packet away from the surface crossing region following the initial passage through this region.

It is interesting to note that the observation of vibrational coherence in a product mode does not necessarily imply that motion is prepared coherently in the excitation process. In a previous paper, we showed that in one-dimensional systems where the time scale of the electronic tunneling interaction is shorter than the vibrational period, the nonadiabatic process can lead to a vibrationally coherent product even when no coherence exists in the reactant state. This is also evident from recent experimental studies. For example, in their studies of the photolysis of the myoglobin–nitric oxide complex, Zhu et al. found that rapid passage of the system through the surface crossing region along the dissociative Mb–NO coordinate produces the ground-state myoglobin vibrationally coherent in both the iron–histidine and heme-doming motions, even though the former mode is not displaced on photoexcitation and thus is not prepared coherently in the pump process.[11]

The experiments discussed above raise some very general and important issues regarding the extent to which the electronic and vibrational dynamics are influenced by the forces acting on the initially prepared wave packet. Relatively little theoretical work on multidimensional nonadiabatic dynamics has been carried out. Jortner and Bixon[38] and Sumi and Marcus[39] have shown the combined effects of intramolecular vibrational motion and diffusive solvent reorientations on the rate of electron-transfer reactions. More recently, Coalson et al.[40] have incorporated excitation effects into a nonequilibrium Golden Rule description of nonadiabatic electron transfer. Cho and Silbey have presented a generalized expression for the nonequilibrium rate of photoinduced electron transfer for a two-dimensional solvation coordinate model, in which the effect of the optical preparation step is explicitly treated.[41] Matro and Cina have recently calculated the femtosecond fluorescence anisotropy arising from excitation transfer between strongly coupled chromophore pairs in which each chrompophore is coupled to a low-frequency vibration.[32] Their results showed that the dissipative nuclear dynamics has a pronounced effect on the form of the anisotropy decay. These authors also discussed the role of intrachromophore vibrational dynamics in determining the dependence of the time-resolved anisotropy on experimental factors such as the excitation pulse width and detection window duration.

In this paper, we treat the situation in which an electronically nonadiabatic process couples to two underdamped vibrational degrees of freedom. These may represent, for example, low-frequency intramolecular modes or specific motions of the surrounding medium that experience strong coupling to the system electronic states. Specifically, we present results from numerical solutions of the multilevel Redfield equations that examine how the electronic population dynamics and product vibrational dynamics are influenced by the extent to which the Franck–Condon active modes project onto the reactive motion.

## Theory

Redfield theory provides a framework for computing the quantum dynamics of a system consisting of a few degrees of freedom interacting with a thermal bath.[42] A detailed formulation of the theory in the context of the electronic curve crossing problem has been presented previously,[28,30] and thus here we briefly review the basics of this approach. The total Hamiltonian has the form

$$H = H_S + H_B + H_{SF} + V \qquad (1)$$

where $H_S$ is the Hamiltonian for the system, $H_B$ is the bath Hamiltonian, and $H_{SF}$ is the interaction between the system degrees of freedom and the external electromagnetic field. $V$ is the system−bath interaction, which introduces energy relaxation and pure dephasing into the system. Treating this interaction to second order and assuming that the bath correlation time, $\tau_c$, is faster than any system relaxation time leads to the Redfield equations for elements of reduced density matrix of the system.

$$\dot{\rho}(t) = \frac{-i}{\hbar}[H_S + H_{SF}, \rho(t)] + R\rho(t) \qquad (2)$$

The dissipative dynamics arising from the system−bath coupling are contained within the Redfield relaxation tensor, $R$. Elements of this tensor describe the damping of populations and coherences within the system and have the form

$$R_{NM,PQ} = \Gamma^{+}_{QM,NP} + \Gamma^{-}_{QM,NP} - \delta_{QM} \sum_S \Gamma^{+}_{NS,SP} - \delta_{NP} \sum_S \Gamma^{-}_{QS,SM} \qquad (3)$$

We assume the system−bath interaction has the form

$$V = \sum_i f_i F_i(\underline{q}) G_i(\underline{Q}) \qquad (4)$$

where $q$ and $Q$ denote the bath and system coordinates, respectively. The constants, $f_i$, are the coupling strengths between system variable $G_i$ and the bath. The terms appearing in eq 3 then have the form

$$\Gamma^{+}_{QM,NP} = \hbar^{-2} \sum_j \sum_j f_i f_j \langle Q|G_i|M\rangle \langle N|G_j|P\rangle \int_0^\infty d\tau\, e^{-i\omega_{NP}\tau} \langle F_i(\tau) F_j(0)\rangle_B$$

$$\Gamma^{-}_{QM,NP} = \hbar^{-2} \sum_i \sum_j f_i f_j \langle Q|G_i|M\rangle \langle N|G_j|P\rangle \int_0^\infty d\tau\, e^{-i\omega_{NP}\tau} \langle F_i(0) F_j(\tau)\rangle_B \qquad (5)$$

Assuming the correlation functions have the form $\langle F_i(\tau)F_j(0)\rangle = \delta_{ij}\, e^{-\tau/\tau_c}$ and that the correlation time, $\tau_c$, is shorter than both the system relaxation times and the system Bohr periods allows the Redfield tensor elements to be written as follows.

$$\Gamma^{+}_{QM,NP} = \hbar^{-2} \sum_i f_i^2 \tau_c\, (1 + e^{\pm\beta\hbar\omega_{NP}})^{-1} \langle Q|G_i|M\rangle \langle N|G_j|P\rangle \qquad (6)$$

The solution to eq 2 can be written formally as $\rho(t) = e^{Lt}\rho(0)$, where $L$ is the Liouville operator. In our previous work, this set of coupled equations was solved in the system eigenstate basis via numerical diagonalization of $L$. For a system with $N$ basis states, the Liouville tensor has $N^2$ elements. The direct diagonalization algorithm scales $N^6$ in this case; thus this method is only feasible for systems containing a few electronic states coupled to, at most, a single vibrational degree of freedom.

Recently, however, a significant advance in density matrix propagation was made by Pollard and Friesner,[33,34] who showed that when the system−bath coupling has the form of eq 4, the time-dependent reduced density matrix can be determined without explicit construction of the full Redfield tensor. Their method, based on the short-iterative Arnoldi procedure,[43,44] generates an approximate propagator at each time step in an $n$-dimensional Krylov subspace spanned by $n - 1$ applications of the Liouville operator to the density matrix. As shown by Pollard and Friesner in several numerical applications of this procedure, the size of the Krylov subspace necessary to converge the results is typically 10−20, independent of the size of the vibronic basis.[34] The maximum time interval during which the propagator is used is chosen such that the density matrix maintains an arbitrarily small projection outside of the $n$-dimensional Krylov subspace. This procedure allows substantial savings in memory and time over propagation via direct diagonalization and standard time-stepping (Runge−Kutta) algorithms, thus making possible application of Redfield theory to systems with a large manifold of states.

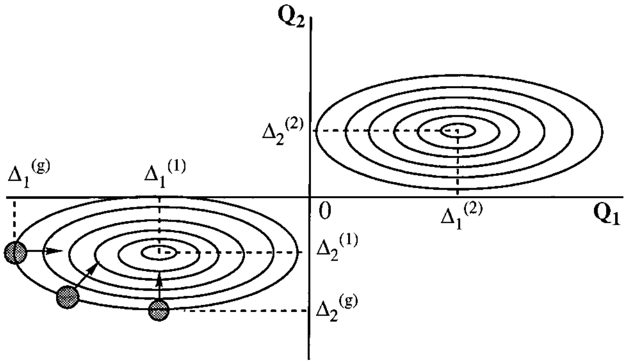

**Figure 2.** Two-dimensional diabatic surfaces for the reactant (1) and product (2) states. $\Delta_i^{(l)}$ is the dimensionless displacement of the $l$th surface along the $i$th vibrational coordinate. The approximate position of the initially excited wave packet for each of the three sets of ground-state displacements are shown.

Pollard and Friesner have pointed out that their formulation of the Redfield equations, which makes possible application of the short-iterative Arnoldi propagation scheme, is similar to the density matrix equation of motion that appears in the axiomatic semigroup theory of Lindblad, Gorini, and co-workers.[45,46] While both treat the system−bath interaction to second order, the latter theory guarantees that the time-evolving density matrix remains positive definite, which is not true of the Redfield equations. At issue is the factorization of the initial density operator into a product of system and bath operators, which neglects transient correlations that must be present for times on the order of the bath correlation time. This has been discussed by a number of authors.[47−50] The neglect of memory effects limits the number of physical reduced density matrices that will remain positive definite during evolution. Suarez et al.[50] have shown that slight modification of the initial conditions is sufficient to ensure positivity during evolution under the Redfield equations of motion. Practically speaking, deviations from positivity are limited.

## Model and Numerical Implementation

In this paper, we present results from a series of simulations of electronic surface crossing dynamics in simple two-mode model systems, taking into account the relative positions of the ground- and reactant excited-state potential surfaces. The model is summarized pictorially in Figure 2. The system Hamiltonian is

$$H_S = |g\rangle H_g \langle g| + |1\rangle H_1 \langle 1| + |2\rangle H_2 \langle 2| + J\{|1\rangle\langle 2| + |2\rangle\langle 1|\} \qquad (7)$$

where $H_g$, $H_1$, and $H_2$ are vibrational Hamiltonians for the ground, reactant, and product diabatic states, respectively. $J$ is the electronic tunneling interaction between the excited diabatic surfaces and is assumed to be independent of the nuclear coordinates. We choose the system modes to be harmonic and consider only linear displacements between the surfaces. Taking the origin of the coordinate system to be the transition state for the curve crossing process, the ground (g), reactant, and product excited-state $l$ vibrational Hamiltonians, expressed in dimensionless normal coordinates, $Q_i$, and momenta, $P_i$, are

$$H_l = \epsilon_l + \frac{1}{2}\{P_1^2 + Q_1^{(l)^2}\}\hbar\omega_1 + \frac{1}{2}\{P_2^2 + Q_2^{(l)^2}\}\hbar\omega_2 \qquad (l = g, 1, 2) \quad (8)$$

where $Q_i^{(l)} = Q_i - \Delta_i^{(l)}$ with $\Delta_i^{(l)}$ denoting the dimensionless displacement of the $l$th surface from the origin along the $i$th coordinate (see Figure 2). We will denote the displacement between reactant ($|1\rangle$) and product ($|2\rangle$) surfaces along the $i$th vibrational coordinate as $\Delta_i^{(1,2)}$ ($= \Delta_i^{(2)} - \Delta_i^{(1)}$) and the displacement between ground ($|g\rangle$) and reactant ($|1\rangle$) surfaces along the $i$th coordinate as $\Delta_i^{(g,1)}$ ($= \Delta_i^{(1)} - \Delta_i^{(g)}$). The reorganization energy, which is the potential energy difference between the reactant and product equilibrium positions in the product well, is thus $\lambda = {}^1/_2\Delta_1{}^{(1,2)^2}\hbar\omega_1 + {}^1/_2\Delta_2{}^{(1,2)^2}\hbar\omega_2$. The Franck–Condon energy for the $|g\rangle \rightarrow |1\rangle$ optical transition, which is the potential energy difference in the reactant well between ground state and reactant equilibrium positions, is $E_{FC} = {}^1/_2\Delta_1{}^{(g,1)^2}\hbar\omega_1 + {}^1/_2\Delta_2{}^{(g,1)^2}\hbar\omega_2$. $\epsilon_l$ is the vertical energy separation between the ground-state and $l$th excited-state surface ($\epsilon_g = 0.0$), so the electronic origin for $|g\rangle \rightarrow |1\rangle$ occurs at an energy of $E = \epsilon_l - E_{FC}$.

The coupling between the diabatic vibronic states and the thermal bath is obtained by assuming the interaction is diagonal in the electronic index and expanding the interaction about the minimum of each diabatic surface to second order in the system coordinates.[28] Furthermore, we assume perfect correlation among the bath motions interacting with each system mode in each diabatic state. In the diabatic representation, the coupling Hamiltonian has the form

$$V = \sum_{l=1,2} |l\rangle[\sum_{m=1,2} f_m^{(l)} Q_m^{(l)} + g_m^{(l)} Q_m^{(l)}2]\langle l|\cdot F(t) \qquad (9)$$

where $m$ is the vibrational mode index. The terms linear in $Q$ give rise to one-quantum vibrational relaxation. The quadratic terms give rise to two-quantum relaxation processes and pure dephasing. $F(t)$ represents the fluctuating force of the bath modes.

We assume only excited state $|1\rangle$ is optically accessible from the ground state; hence the system-field interaction is given by

$$H_{SF} = -\mu\{|g\rangle\langle 1| + |1\rangle\langle g|\}\cdot E_0 \cos(\omega t)\, e^{-t^2/\tau^2} \qquad (10)$$

with $\mu$ denoting the transition dipole matrix element for the $|g\rangle \rightarrow |1\rangle$ transition and $E_0$, $\omega$, and $\tau$ denoting the electric field amplitude, center frequency, and pulse width of the excitation pulse. The initial excited state in our simulations is obtained by starting with a thermal density matrix for the ground state and solving eq 2 to second order in $H_{SF}$, neglecting the effects of dissipation during the pulse.

While the diabatic states provide a convenient basis in which to formulate the surface crossing problem, solution of the Redfield equations is carried out in the representation of eigenstates of the system Hamiltonian.[28] The ground electronic state enters into our problem only during the optical preparation step, thus following the initial preparation step, we carry out the subsequent dynamics in the basis of eigenstates of $H_{ex,}$ where $H_{ex} = |1\rangle H_1\langle 1| + |2\rangle H_2\langle 2| + J\{|1\rangle\langle 2| + |2\rangle\langle 1|\}$. The eigenstates can be written as $|N\rangle = \Sigma_{l;i,j} C_{l;i,j}^{(N)}|l;i,j\rangle$ where $l = 1$ or 2 and $i$ and $j$ refer to vibrational quantum numbers. $C_{l,i,j}^{(N)}$ is the projection of eigenstate $|N\rangle$ onto the diabatic vibronic state $|l;i,j\rangle$. The size of the vibronic basis set depends on the normal mode displacements, temperature, etc. Time-dependent populations of the reactant diabatic state, $P^{(1)}(t)$, are calculated by transforming the density matrix in the eigenstate representation back to the diabatic representation and tracing over only those states that belong to the reactant manifold. The average values of the nuclear coordinates for population in excited state $l$ are calculated from the appropriate diabatic density matrix, $p_{(t)}^{(l)}$, by

$$\langle Q_m^{(l)}(t)\rangle = \mathrm{Tr}\{p_{(t)}^{(l)}\, Q_m^{(l)}\} \qquad (11)$$

For the results presented here, typically 18–20 basis states per mode per excited state (i.e., 648–800 states total) were used to calculate the system eigenstates. The short-iterative Arnoldi propagation routine was used with a 25-dimensional Krylov subspace. The length of each time step was restricted by placing a maximum projection of the final density matrix outside of the Krylov space of $10^{-8}$. The number of basis states, the cutoff parameter, and the size of the Krylov subspace were varied in order to ensure convergence of the results.

## Results and Discussion

In this section, we present results from simulations that examine how the initial position of and force acting on the reactant wave packet influence the subsequent curve crossing dynamics in a two-mode double well. As noted earlier, this depends on both the excited-state displacements and the spectral and temporal properties of the excitation pulse. In this paper, we focus solely on the effect of varying the displacements between the ground and reactant and product excited-state surfaces. A thorough discussion of the dependence of excited-state dynamics on excitation pulse frequency has been presented by Matro and Cina.[32]

The normal mode displacements between the ground and reactant and product excited states were chosen in such a way that the total Franck–Condon and reorganization energies for the different calculations were held constant. This allowed variation of the location of the Franck–Condon region, while keeping the amount of excess vibrational energy deposited in the pump process and barrier height between the wells constant. Unless stated otherwise, we take the energy bias between the wells to be zero (i.e., symmetric double well). The initial position and initial force acting on the wave packet is governed by the displacements, $\Delta_i^{(g,1)}$, between the ground and excited reactant surfaces. For $\Delta_i^{(g,1)} = 0$, impulsive excitation results in a spatial probability distribution for that mode that is thermal. With increasing displacement, the number of Franck–Condon transitions accessible from a given ground-state level increases, with the result that the initial wave packet becomes increasingly displaced (relative to the excited-state minimum) along the $i^{th}$ coordinate.

The two vibrational modes are chosen to have frequencies of 80 and 200 cm$^{-1}$, which have periods of 417 and 167 fs, respectively. The center frequency of the excitation pulse was held fixed at 500 cm$^{-1}$ above the electronic origin. The temporal width of the pulse (10 fs) corresponds to a coherent bandwidth sufficient to span approximately 5–10 levels of each mode. The thermal energy, $kT$, is 200 cm$^{-1}$ (T = 288 K) and the system–bath coupling terms, $f_i^2\tau_c$ and $g_i^2\tau_c$, for each mode were chosen such that the population relaxation and pure dephasing times for the 1 → 0 vibrational transition in each diabatic state were 2.60 and 5.30 ps, respectively.

Our model is similar to that employed by Matro and Cina in their application of Redfield theory to electronic energy transfer in a model for a strongly coupled photosynthetic dimer;[32] however, there are some important differences that merit mention. Matro and Cina assumed the ground state to be fixed at the position $Q_1 = 0.0$, $Q_2 = 0.0$ with the positions of the excited-state minima symmetrically displaced from the origin. Additionally, they allowed optical access to one or both monomer excited states and investigated the effects of transition dipole orientation and the noninstantaneous nature of the pump and detection events on the time-resolved emission anisotropy. In this paper, we focus on the effects of varying the relative displacements of the three states for a given excitation center frequency and temporal duration on the electronic population and vibrational dynamics directly.

Simulations were carried out for both strong and weak electronic coupling for two different reaction coordinates, which vary in the extent to which the two modes couple to the curve crossing process. The first set of results we discuss pertain to a model in which $\Delta_1^{(1,2)} = 4.24$ and $\Delta_2^{(1,2)} = 0.0$, so that only the lower frequency motion is reactive. The reorganization energy is 720 cm$^{-1}$. The tunneling splitting of the surfaces ($2J$) is 50 cm$^{-1}$, so that the barrier height is 155 cm$^{-1}$, which is slightly less than $kT$. The time-dependent nonequilibrium population of the initial state is shown in Figure 3a for three different sets of reactant excited-state displacements:

(i) $\Delta_1^{(g,1)} = 3.16$; $\Delta_2^{(g,1)} = 0.00$ (only the 80 cm$^{-1}$ mode is Franck–Condon active), (ii) $\Delta_1^{(g,1)} = 2.10$; $\Delta_2^{(g,1)} = 1.50$ (both modes are Franck–Condon active), and (iii) $\Delta_1^{(g,1)} = 0.0$; $\Delta_2^{(g,1)} = 2.00$ (only the 200 cm$^{-1}$ mode is Franck–Condon active). In each case the Franck–Condon energy is 400 cm$^{-1}$, thus the average energy of the initially prepared wave packet is $\sim kT$ above the barrier.

For the two excitation cases where the reactive mode is also Franck–Condon active, the wave packet is prepared such that a substantial component of the initial force it experiences is directed toward the crossing region. The dephasing rates are such that the nuclear motion in the reactant well is underdamped, as can be seen in Figure 3b, which shows the average values of the two system coordinates for case (ii), where both modes are prepared coherently.

The decay of the nonequilibrium population of the reactant state for these two cases occurs on similar time scales. However, in the case where only the reactive motion is coherently excited, periodic sampling of the crossing region by the localized wave packet occurs, which gives rise to stepwise decay of the reactant population ("quantum plateaus"). Stepwise decay has been observed in the experiments of Scherer et al.[4] on the solvent-induced predissociation of $I_2$ and in calculations on the same system by Ben-Nun et al.[5] In that system, two dissociation events per vibrational period were observed, one each on the outgoing and incoming trajectories. In the example shown here, we observe only one plateau per period due to the fact that the fraction of the wave packet that remains on the reactant surface following passage through the crossing region has insufficient energy to move completely out of the crossing region. The proximity of the surface crossing and classical turning point causes the outgoing and incoming plateaus to blend together. Dephasing interactions with the bath tend to wash out the stepwise effect as can be seen from the long time behavior of the decay. The observed step depth and periodicity (417 fs) of the population drop-offs provides a direct measure of both the single passage surface crossing probability and the frequency of the reactive motion. The presence of a second coherently prepared mode with a different vibrational period has the effect of further obscuring the quantum plateaus, even though the motion of the wave packet on the reactant surface is still underdamped in both modes for several picoseconds. When only the nonreactive (200 cm$^{-1}$) mode is Franck–Condon active, the force acting on the wave packet is perpendicular to the reaction coordinate. In this case, a markedly slower rate of reaction is observed and the decay of the reactant-state population is monotonic.

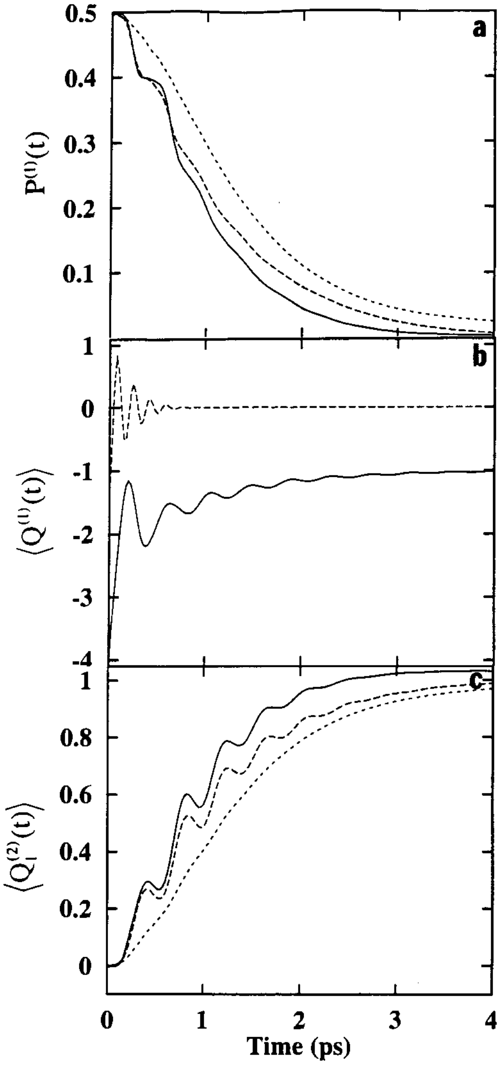

**Figure 3.** Effect of ground-state position on photoinduced curve crossing dynamics in a two-mode symmetric double well with $\Delta_1^{(1,2)} = 4.24$, $\Delta_2^{(1,2)} = 0.0$, and $J = 25$ cm$^{-1}$. (—) $\Delta_1^{(g,1)} = 3.16$, $\Delta_2^{(g,1)} = 0.0$; (- - -) $\Delta_1^{(g,1)} = 2.10$, $\Delta_2^{(g,1)} = 1.50$; (···) $\Delta_1^{(g,1)} = 0.0$, $\Delta_2^{(g,1)} = 2.00$. (a) Nonequilibrium reactant-state population. (b) Average values of the vibrational coordinates $Q_1(t)$ and $Q_2(t)$ in the reactant state for excitation case (ii). (c) Average value of the coordinate $Q_1(t)$ in the product state for the three excitation conditions.

It is interesting to examine the nature of nuclear motion in the product well in the case where the electronic coupling is sufficiently weak that only a small fraction of the reactant population decays on each visit to the crossing region. Figure 3c shows the average value of the reaction coordinate for that fraction of the population that is in the product electronic state (i.e., $\langle Q_1^{(2)}(t) \rangle$) for the three excitation conditions. For the two cases where the reaction coordinate is prepared coherently, the product at early times is formed in a stepwise manner, i.e., a new wave packet is launched on the product surface every 417 fs. Each new wave packet has a well-defined phase relationship with the previously launched wave packet. The resulting amplitude interference between these wave packets explains the simple periodicity seen in the average value of $Q_1$. In a model where the vibrational frequencies of the reactant and product wells differed, the lack of constructive interference between wave packets launched at different times would lead to a considerably more complicated behavior for $\langle Q_1^{(2)}(t)\rangle$.

It is useful at this point to note that the time-dependent average displacement of the *i*th system coordinate in the *l*th diabatic state, as defined by eq 11, depends on both the magnitudes of the vibrational coherences (off-diagonal elements of $\text{p}^{(l)}$) and the total population in the *l*th diabatic state (Tr $\text{p}^{(l)}$). The dynamics displayed by $\langle Q^{(l)}{}_i(\text{t})\rangle$ thus are damped not only by vibrational energy transfer to the bath and bath-induced pure dephasing, but also population flow between the reactant and product diabatic wells. To illustrate how population transfer between wells influences the long time values of the coordinates, consider the particular case shown above in Figure 3. Recall that the two wells are displaced symmetrically about the origin. The equilibrium position of the reactant excited state is at $Q_1 = -2.12$, $Q_2 = 0.0$ (i.e., (−2.12, 0.0)). For excitation case (ii), the ground-state displacement parameters ($\Delta_i^{(\text{g},1)}$) correspond to a position of (−4.22, −1.50) for the Franck−Condon region. In the absence of population flow between wells, the trace of the diabatic density matrix of the initially excited state remains constant (i.e., Tr $p^{(1)} = 1$) and the average position at long times would correspond to the equilibrium position (−2.12, 0.0). In the presence of population transfer between wells, the equilibrium population in the reactant well is 0.5 and the long time values for the coordinates are (−1.06, 0.0), as can be seen from eq 11 and the definition of $Q_1^{(1)}$. Thus in Figure 3b the value of $\langle Q_1^{(1)}(t)\rangle$, for example, ranges from −4.28 to −1.06. Likewise, $\langle Q_1^{(2)}(t)\rangle$ (Figure 3c) ranges from 0.0 at $t = 0$ to $+1.06$ at $t = \infty$.

The effect of the location of the Franck−Condon region on the electronic population dynamics in this model is even more pronounced when the electronic coupling is made stronger. Figure 4a shows the decay of the reactant population for the same three excitation conditions and system−bath coupling parameters used previously; however, this time the tunneling splitting is 160 cm$^{-1}$. Again we see that coherent preparation of the reactive mode leads to significant enhancement of the decay rate compared to the case where this mode is prepared thermally. In these cases, the vast majority of the nonequilibrium population becomes product during the first traversal of the crossing region.

In the stronger electronic coupling case, oscillations are observed in the population dynamics at approximately 0.6 and 1.1 ps when the reaction coordinate is coherently excited. These features result from coherent vibrational motion that survives the curve crossing process, giving rise to underdamped wave packet motion on the product surface. The product well dynamics are shown in Figures 4b and 4c. Since the dephasing time in the product well is longer than the vibrational period, the wave packet can revisit the crossing region leading to coherent recrossings of the barrier. Note that for the case where only the 200-cm$^{-1}$ vibration is coherently prepared, the coherent motion of this mode seen in the product well does not lead to coherent recrossings since the momentum is directed perpendicular to the crossing region.

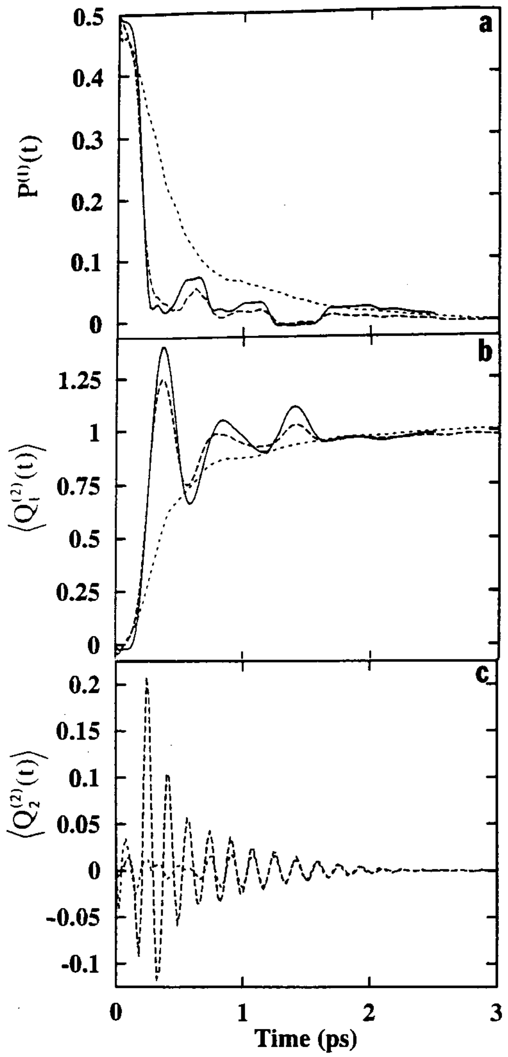

**Figure 4.** Effect of ground-state position on photoinduced curve crossing dynamics in a two-mode symmetric double well with $\Delta_1^{(1,2)} = 4.24$, $\Delta_2^{(1,2)} = 0.0$, and $J = 80$ cm$^{-1}$. (—) $\Delta_1^{(\text{g},1)} = 3.16$, $\Delta_2^{(\text{g},1)} = 0.0$; (- - -) $\Delta_1^{(\text{g},1)} = 2.10$, $\Delta_2^{(\text{g},1)} = 1.50$; (···) $\Delta_1^{(\text{g},1)} = 0.0$, $\Delta_2^{(\text{g},1)} = 2.00$. (a) Nonequilibrium reactant-state population. (b) Average values of the vibrational coordinate $Q_1(t)$ in the product state. (c) Average values of the coordinate $Q_2(t)$ in the product state.

It is interesting to compare the dynamics of the higher frequency (nonreactive) mode in the product state for the two cases where this mode is prepared coherently (Figure 4c). The magnitude of the coherence seen in the product state is substantially greater when the lower frequency mode is also coherently excited. The reason for this is that coherent preparation of the reaction coordinate leads to much faster population transfer between wells, thus preserving some localization of the wave packet along the orthogonal direction.

In the previous set of examples, the lower frequency mode corresponded to the reaction coordinate and the higher frequency motion served as a spectator mode. The next set of results we discuss pertains to a system where both vibrational modes couple to the curve crossing process. We choose the displacements between the reactant and product surfaces to be $\Delta_1^{(1,2)} = 3.00$; $\Delta_2^{(1,2)} = 1.90$, which, as in the previous scenario, yields a reorganization energy of $\lambda = 720$ cm$^{-1}$. We consider only the stronger electronic coupling case, i.e., $2J = 160$ cm$^{-1}$. The population dynamics for the three excitation conditions are shown in Figure 5. Here, each excitation condition generates a wave packet on the upper surface that experiences a significant

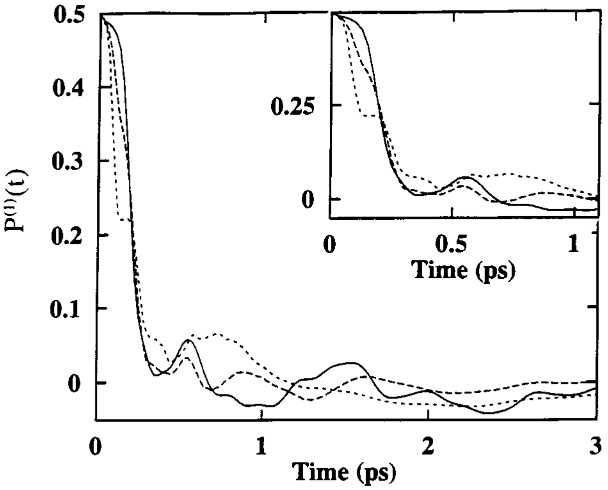

**Figure 5.** Effect of ground-state position on nonequilibrium reactant population dynamics in a two-mode symmetric double well with $\Delta_1^{(1,2)} = 3.00$, $\Delta_2^{(1,2)} = 1.90$, and $J = 80$ cm$^{-1}$. (—) $\Delta_1^{(g,1)} = 3.16$, $\Delta_2^{(g,1)} = 0.0$; (- - -) $\Delta_1^{(g,1)} = 2.10$, $\Delta_2^{(g,1)} = 1.50$; (···) $\Delta_1^{(g,1)} = 0.0$, $\Delta_2^{(g,1)} = 2.00$. Inset: short time population dynamics showing the first passage through the crossing region and first recurrence.

force directed toward the crossing region. In each case, >90% of the nonequilibrium population has decayed within ~250 fs; however, both the short time and long time dynamics show some dependence on the initial position of the wave packet. The short time (<300 fs; see inset of Figure 5) behavior clearly shows that the fraction of reactant population that becomes product on the first passage through the crossing region depends sensitively on the geometry of the approach of the wave packet to the crossing region. For example, for the cases where the more strongly displaced 80-cm$^{-1}$ mode is prepared coherently, virtually all of the nonequilibrium population is lost in approximately half of the vibrational period (210 fs).

For the case where the only the 200-cm$^{-1}$ mode is prepared coherently, we again see stepwise decay of the reactant population with only half of the nonequilibrium population lost during the first passage through the crossing region.

The magnitude and frequency of the coherent recrossings also depend on the force acting on the initial wave packet. For the two cases in which the lower frequency mode is prepared coherently, a sharp recurrence in the population dynamics occurs at approximately 550 fs (~1.5 vibrational periods). In the case where only the higher frequency mode is coherently excited, the decay shows a considerably broader recurrence at ~750 fs. The differences in the nature of the recurrences can be understood by examining the product well vibrational dynamics shown in Figure 6. Regardless of whether one or both modes are coherently excited, passage of the wave packet through the crossing region occurs rapidly enough to produce a wave packet that is localized to some extent along both coordinates in the product well. Thus, in each case, we see some coherent motion in both vibrational modes in the product state. Consider the two cases in which the 80-cm$^{-1}$ mode is coherently prepared. For a coherent barrier recrossing to occur, both vibrations must arrive back at the crossing region at the same time. Whether or not this occurs depends on the phase relation between the two vibrations. For example, it is seen in Figure 6a that for the case where only the 80-cm$^{-1}$ vibration is Franck–Condon active the phase relation between the two product vibrations is such that each is approaching the crossing region at ~0.55 ps, resulting in a favorable momentum for crossing back to the reactant well. In the case where both vibrations are Franck–Condon active (Figure 6b), the wave packet traverses the crossing region along a different trajectory than before, with the result that the phase relation between the two modes is no longer such that both motions arrive back at the crossing region at the same time. This has the effect of diminishing the flow of population back to the reactant well as compared to the previous case. The situation appears to be somewhat more complicated in the case where only the 200-cm$^{-1}$ mode is prepared coherently (Figure 6c). Here, the fraction of the wave packet launched on the product surface is considerably reduced compared to the other cases, and the reactant wave packet samples the crossing region more often in the first few hundred femtoseconds. This results in two partially localized wave packets appearing on the product surface during the first 250–300 fs. The resulting amplitude interference between these two wave packets in the product well accounts for the smearing out of the recurrence seen in the population dynamics.

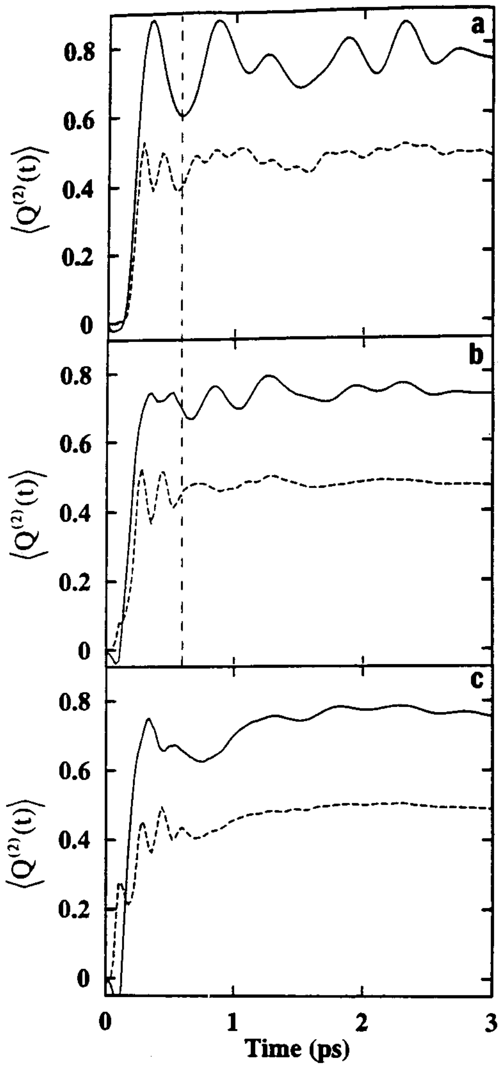

**Figure 6.** Effect of ground-state position on product vibrational dynamics for the two-mode system of Figure 4. (—) $\langle Q_1^{(2)}(t)\rangle$; (- - -) $\langle Q_2^{(2)}(t)\rangle$. (a) $\Delta_1^{(g,1)} = 3.16$, $\Delta_2^{(g,1)} = 0.0$; (b) $\Delta_1^{(g,1)} = 2.10$, $\Delta_2^{(g,1)} = 1.50$; (c) $\Delta_1^{(g,1)} = 0.0$, $\Delta_2^{(g,1)} = 2.00$. The vertical dashed lines in (a) and (b) denote the time of the first sharp electronic recurrence seen in the electronic population dynamics.

It is interesting to note that in the case where only the lower frequency mode is coherently excited, rapid passage through the crossing region produces a product that is coherently excited in the 200-cm$^{-1}$ mode (Figure 6a, dashed line). This is reminiscent of the situation in the photodissociation of the Mb–

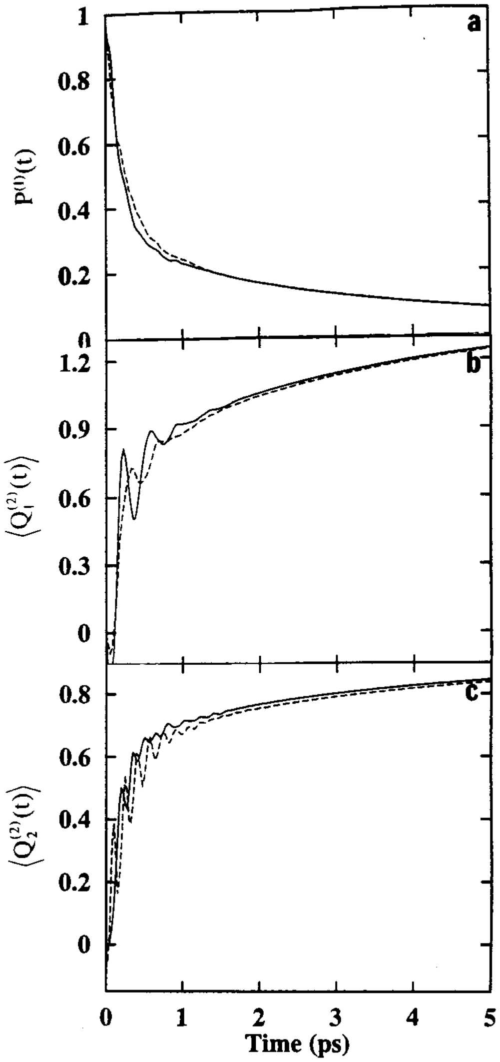

**Figure 7.** Effect of ground-state position on nonequilibrium reactant population dynamics in a two-mode biased double well with $\Delta_1^{(1,2)} = 3.00$, $\Delta_2^{(1,2)} = 1.90$, $J = 80$ cm$^{-1}$, and $\epsilon = 700$ cm$^{-1}$. (—) $\Delta_1^{(g,1)} = 3.16$, $\Delta_2^{(g,1)} = 0.0$; (- - -) $\Delta_1^{(g,1)} = 0.0$, $\Delta_2^{(g,1)} = 2.00$. (a) Nonequilibrium reactant state population. (b) Average values of the vibrational coordinate $Q_1(t)$ in the product state. (c) Average values of the coordinate $Q_2(t)$ in the product state.

NO complex studied by Champion and co-workers,[11] where the myoglobin ground state was produced vibrationally coherent in the iron−histidine stretching motion even though this mode is not Franck−Condon active in the absorption process. As noted above, a significant electronic recurrence is seen in the simulation in this case at 550 fs, which results from the in-phase arrival of the product vibrations to the surface crossing region. No such recurrence is seen in the Mb−NO data since the reactive motion occurs along a dissociative coordinate. Nevertheless, it is significant that we observe coherent motion in a vibrational mode of the product arising from the ultrafast nonadiabatic process.

Next, we examine the effect on the reaction dynamics of introducing an energy bias between the reactant and product wells. We choose the same system discussed in the previous paragraph, except with an energy bias of 700 cm$^{-1}$, which puts the system near the Marcus inverted region. In this case, the wave packet appears on the product surface with several hundred wavenumbers of excess vibrational energy. Figure 7a shows the electronic population dynamics for the cases where only the higher or the lower frequency mode is Franck−Condon active (i.e., excitation conditions (i) and (iii)). The two decays are virtually indistinguishable, and no recurrences are seen in the population dynamics. This is due to rapid energy relaxation in the product well (it is easily shown that the one-quantum energy relaxation rates within a diabatic state scale as the vibrational quantum number[51]). This effectively traps the system in the product well, preventing any electronic recurrences. The product vibrational dynamics for these cases are shown in Figures 7b and 7c. Note that despite the rapid loss of excess vibrational energy in the product well to the bath, the vibrations continue to oscillate for several periods. This behavior arises from coherence transfer processes, which have been shown to lead to damping times for vibrational modes that exceed energy relaxation times.[30,31]

Finally, we discuss the relevance of some of the ideas presented here to the detailed studies of the primary photochemical process occurring in the rhodopsin system.[15−18,27] This work, in particular, shows how the preparation and detection of coherent vibrational wave packets can be used to gain detailed insight into reactive trajectories. In these experiments, the trans photoproduct was found to form irreversibly in <200 fs following excitation. Furthermore, the product was found to be produced vibrationally coherent in a 60-cm$^{-1}$ mode assigned to the reactive skeletal torsion. The damping time of the torsion in the product state was found to be ~2 ps. As mentioned earlier, this mode is strongly Franck−Condon active in the 11-*cis*-retinal chromophore due to the steric interaction between the 13-methyl group and 10-hydrogen atom. Thus, femtosecond excitation results in a wave packet localized along the torsional direction, which rapidly directs the system out of the Franck−Condon region and through the crossing region in the absence of phase-destroying collisions. Interestingly, these authors find that the photoisomerization process in 13-demethylrhodopsin, which is missing the nonbonded interaction with the 10-hydrogen, occurs a factor of >2 more slowly, leading them to conclude that the large displacement along the reaction coordinate between the ground and excited surfaces of the 11-cis pigment accounts for the rapid rate and high quantum yield for isomerization in rhodopsin.[18] This conclusion is supported by the simulation results discussed above, which show that strong Franck−Condon activity in a mode with a large projection onto the reaction coordinate leads to an acceleration of the curve crossing process and coherent vibrational dynamics in the product state.

A second interesting aspect of the rhodopsin experiments is the lack of observation of electronic recurrences in the population dynamics, even though the trans product continues to vibrate coherently for ~2 ps. In a previous paper,[31] we reported simulation results from a simple one-mode model for the isomerization process in rhodopsin, which showed that the absence of electronic recurrences could be explained by efficient coherence transfer processes, which allowed fast energy relaxation, thus trapping the wave packet in the product well, without complete destruction of vibrational phase coherence. Alternatively, multimode mode effects may play an important role in explaining the lack of electronic recurrences. The resonance Raman spectrum of the 11-cis isomer shows strong Franck−Condon displacements in several low-frequency modes.[52] A multimode analysis of the resonance Raman intensities, as well as the excited-state dynamic absorption and emission spectra, shows that the majority of the Franck−Condon energy arises from displacements in intramolecular modes.[27] The 30-fs pump pulse used by Mathies et al. in their photoisomerization experiments is sufficient to coherently excite several of these motions. The extent to which coherent motion in modes other than the skeletal torsion persists through the curve crossing process is unclear. Results from our two-mode model systems show that the product of an ultrafast curve crossing process can be produced vibrationally coherent regardless of whether the vibration is coupled to the electronic process. The observation of a single coherent mode in the trans product may result from either rapid damping of the other motions prior to passage through the crossing region or from a lack of Franck−Condon activity of these motions in the probe process, in which case coherent vibrational motion would not influence the time-resolved spectrum. If the trans photoproduct is produced vibrationally coherent in more than one mode, then the time it takes the wave packet to revisit the crossing region may be longer than the 2-ps dephasing time. This latter scenario does not rely on ultrafast energy relaxation of the trans product.

## Conclusions

The results from this study clearly show that the competition between coherent vibrational motion and energy and phase relaxation in ultrafast photoinduced electronically nonadiabatic processes leads to electronic and nuclear dynamics that depend sensitively on the location of and force acting on the initially prepared wave packet. In the case of a symmetric double well, for given values of the Franck−Condon and reorganization energies, the electronic population dynamics, as well as the product vibrational dynamics, were found to depend on the extent to which the Franck−Condon active modes couple to the nonadiabatic process.

For weak electronic coupling, where barrier recrossings are unimportant, coherent motion along modes with significant projections onto the reactive motion leads to repetitive sampling of the crossing region and stepwise decay of the reactant. As the number of underdamped Franck−Condon active modes increases, this effect washes out, with the result that the decay of the nonequilibrium population in the initially excited state becomes monotonic. For the strong electronic coupling case, where a substantial fraction of the nonequilibrium reactant population becomes product on a single passage through the crossing region, it was found that the dynamics of the initial surface crossing and the magnitude and frequency of coherent recrossings arising from underdamped vibrational motion in the product well depend sensitively on the properties of the intial wave packet.

We note that the model employed here contained only linear displacements between ground- and exctited-state minima. Extension of the model to incorporate quadratic Franck−Condon interactions (frequency shifts, mode mixing) and anharmonic couplings between vibrational modes presents no difficulty. It would be interesting to investigate the effects of anharmonic interactions between the coordinates since these would allow for rapid mode−mode energy exchange. Such processes may have profound influences on the nature of nonadiabatic reactions in which more than one coordinate couples to the electronic transition. In addition, extension of our method to systems with more than two modes and/or more than two electronic states is feasible, given the computational efficiency of the short-iterative Arnoldi propagation scheme of Pollard and Friesner.

**Acknowledgment.** The author would like to thank Professors Jeffrey Cina, Graham Fleming, and David Jonas for useful discussions during the preparation of this manuscript and Dr. W. T. Pollard and Professor Richard Friesner for making available their density matrix propagation code.

## References and Notes

(1) Domcke, W.; Stock, G. *Adv. Chem. Phys.* **1997**, *100*, 1.
(2) Fleming, G. R.; Joo, T.; Cho, M. *Adv. Chem. Phys.*, in press.
(3) Tanimura, Y.; Mukamel, S. *J. Chem. Phys.* **1994**, *101*, 3049.
(4) Scherer, N. F.; Jonas, D. M.; Fleming, G. R. *J. Chem. Phys.* **1993**, *99*, 153.
(5) Ben-Nun, M.; Levine, R. D.; Jonas, D. M.; Fleming, G. R. *Chem. Phys. Lett.* **1995**, *245*, 629.
(6) Zadoyan, R.; Li, Z.; Ashjian, P.; Martens, C. C.; Apkarian, V. A. *Chem. Phys. Lett.* **1994**, *208*, 504.
(7) Zadoyan, R.; Li, Z.; Martens, C. C.; Apkarian, V. A. *J. Chem. Phys.* **1994**, *101*, 6648.
(8) Kliner, D. A. V.; Alfano, J. C.; Barbara, P. F. *J. Chem. Phys.* **1993**, *98*, 5375.
(9) Ashkenazi, G.; Banin, U.; Bartana, A.; Kosloff, R.; Ruhman, S. *Adv. Chem. Phys.* **1997**, *100*, 229.
(10) Schwartz, B. J.; King, J. C.; Zhang, J. Z.; Harris, C. B. *Chem. Phys. Lett.* **1993**, *203*, 503.
(11) Zhu, L.; Sage, J. T.; Champion, P. M. *Science* **1994**, *266*, 629.
(12) Pugliano, N.; Palit, D. K.; Szarka, A. Z.; Hochstrasser, R. M. *J. Chem. Phys*. **1993**, *99*, 7273.
(13) Wynne, K.; Reid, G. D.; Hochstrasser, R. M. *J. Chem. Phys.* **1996**, *105*, 2287.
(14) Wynne, K.; Galli, C.; Hochstrasser, R. M. *J. Chem. Phys.* **1994**, *100*, 4797.
(15) Peteanu, L. A.; Schoenlein, R. W.; Wang, Q.; Mathies, R. A.; Shank, C. V. *Proc. Natl. Acad. Sci. U.S. A.* **1993**, *90*, 11762.
(16) Wang, Q.; Schoenlein, R. W.; Peteanu, L. A.; Mathies, R. A.; Shank, C. V. *Science* **1994**, *266*, 422.
(17) Kochendoerfer, G. G.; Mathies, R. A. *J. Phys. Chem.* **1996**, *100*, 14526.
(18) Wang, Q.; Kochendoerfer, G. G.; Schoenlein, R. W.; Verdegem, P. J. E.; Lugtenberg, J.; Mathies, R. A.; Shank, C. V. *J. Phys. Chem.* **1996**, *100*, 17388.
(19) Bradforth, S. E.; Jiminez, R.; van Mourik, F.; van Grondelle, R.; Fleming, G. R. *J. Chem. Phys.* **1995**, *99*, 16179.
(20) Chachisvilis, M.; Pullerits, T.; Jones, M. R.; Hunter, C. N.; Sundstrom, V. *Chem. Phys. Lett.* **1994**, *224*, 345.
(21) Vos, M. H.; Lambry, J.-C.; Robles, S. J.; Youvan, D. C.; Breton, J.; Martin, J.-L. *Proc. Natl. Acad. Sci. U.S.A.* **1991**, *88*, 8885.
(22) Vos, M. H.; Rappaport, F.; Lambry, J.-C.; Breton, J.; Martin, J.-L. *Nature* **1993**, *363*, 320.
(23) Stanley, R. J.; Boxer, S. G. *J. Phys. Chem.* **1995**, *99*, 859.
(24) Marcus, R. A.; Sutin, N. *Biochim. Biophys. Acta* **1985**, *811*, 265.
(25) Onuchic, J. N.; Wolynes, P. G. *J. Phys. Chem.* **1988**, *92*, 6495.
(26) Schatz, G. C.; Ratner, M. A. *Quantum Mechanics in Chemistry*; Prentice Hall: Englewood Cliffs, New Jersey, 1993; Chapter 8.
(27) Wexler, D.; Mathies, R. A. *J. Phys. Chem.*, submitted for publication.
(28) Jean, J. M.; Friesner, R. A.; Fleming, G. R. *J. Chem. Phys.* **1992**, *96*, 5827.
(29) Jean, J. M. *J. Chem. Phys.* **1994**, *101*, 10464.
(30) Jean, J. M.; Fleming, G. R. *J. Chem. Phys.* **1995**, *103*, 2092.
(31) Jean, J. M. *J. Chem. Phys.* **1996**, *104*, 5638.
(32) Matro, A.; Cina, J. A. *J. Phys. Chem.* **1995**, *99*, 2568.
(33) Pollard, W. T.; Felts, A. K.; Friesner, R. A. *Adv. Chem. Phys.* **1996**, *93*, 77.
(34) Pollard, W. T.; Friesner, R. A. *J. Chem. Phys.* **1994**, *100*, 5054.
(35) May, V.; Kuhn, O.; Schreiber, M. *J. Phys. Chem*. **1993**, *97*, 12591.
(36) Kuhn, O.; May, V.; Schreiber, M. *J. Phys. Chem*. **1994**, *100*, 10404.
(37) Bixon, M.; Jortner, J. *J. Chem. Phys.* **1997**, *107*, 1470.
(38) Jortner, J.; Bixon, M. *J. Chem. Phys.* **1988**, *88*, 167.
(39) Sumi, H.; Marcus, R. A. *J. Chem. Phys.* **1986**, *84*, 4894.
(40) Coalson, R. D.; Evans, D. G.; Nitzan, A. *J. Chem. Phys.* **1994**, *101*, 436.
(41) Cho, M.; Silbey, R. J. *J. Chem. Phys.* **1995**, *103*, 595.
(42) Redfield, A. G. *Adv. Magn. Reson.* **1965**, *1*, 1.
(43) Arnoldi, W. E. *Q. Appl. Math.* **1951**, *9*, 17.
(44) Friesner, R. A.; Tuckerman, L. S.; Dornblaser, B. C.; Russo, T. V. *J. Sci. Comput.* **1989**, *4*, 327.
(45) Gorini, V.; Kossakowski, A.; Sudarshan, E. C. G. *J. Math. Phys.* **1976**, *17*, 821.
(46) Lindblad, G. *Commun. Math. Phys.* **1976**, *48*, 119.
(47) Dumcke, R.; Spohn, H. *Z. Phys.* B **1979**, *34*, 419.
(48) Pechukas, P. In *Large Scale Molecular Systems*; Gans, W., Blumen, A., Amann, A., Eds.; Plenum: New York, 1991; p 123.
(49) Alicki, R.; Lendi, K. *Quantum Dynamical Semigroups and Applications*; Springer: Berlin, 1987.
(50) Suarez, A.; Silbey, R.; Oppenheim, I. *J. Chem. Phys.* **1992**, *97*, 5101.
(51) Louisell, W. H. *Quantum Statistical Properties of Radiation*; Wiley: New York, 1973; Chapter 6.
(52) Loppnow, G. R.; Mathies, R. A. *Biophys. J.* **1988**, *54*, 35.